An in-process tool wear evaluation approach for ultra-precision fly cutting

Guoqing Zhang[a,b], Suet To[b,c*]

[a]College of Mechatronics and Control Engineering, Shenzhen University, Shenzhen 518060, PR China

[b]State Key Laboratory of Ultra-precision Machining Technology, Department of Industrial and Systems Engineering, The Hong Kong Polytechnic University, Kowloon, Hong Kong, PR China

[c]Shenzhen Research Institute of The Hong Kong Polytechnic University, Shenzhen, PR China

* Corresponding Author / E-mail: sandy.to@polyu.edu.hk, TEL: +852-2766-6587, FAX: +852-2764-7657

Abstract. Ultra-precision fly cutting (UPFC) is an intermittent cutting process, which is widely used in the fabrication of non-rotational symmetric micro structures with sub-micron form accuracy and nanometric surface roughness. In UPFC, the occurrence of tool wear certainly affects the accuracy of machined micro structures. Aimed at the close relations between tool wear and chip morphologies and the truth that cutting chips are fully formed in a cutting cycle, this research developed a tool wear evaluation approach based on cutting chips. Chip morphology features related to tool failure patterns were identified and then parameterized to predict the tool failure patterns, the surface topography, and surface roughness under the effects of tool failure patterns. Predictions were then verified by experimental results. Research results show that chip morphologies were successfully used to present tool failure pattern, following the well-designed identification procedures, the tool failure patterns are accurately identified. This approach is practical since it can in-process identify tool failure patterns and their effects on surface quality.

Keywords: Tool wear; Cutting chips; Evaluation system; Ultra-precision fly cutting

1 Introduction

Ultra-precision fly cutting (UPFC) is a typical intermittent cutting process, which is widely used in the fabrication of non-rotational symmetric surface structures with high form accuracy and surface finish [1]. However, tool wear occurrence directly affects form accuracy and roughness of the machined surface. In order to reduce the effects of tool wear on the quality of machined surface, tool wear evaluation approaches are widely used. Tool wear evaluation approaches are classified into two categories: direct and indirect approaches [2]. Direct tool wear evaluation approach is conducted directly by visual action, for example, the optical system is the most commonly used system for tool wear evaluation [3]. Visual tool wear evaluation approach can directly find out tool failure patterns. However, it is difficult to be realized online since cutting chips cover the cutting tool during the cutting. Indirect tool wear evaluation approach is realized by using indirect cutting signals [4-5], which can be conducted both online and in real-time, however, it fails to identify the tool failure patterns exactly.

Cutting chips are directly generated from the material removal processes in metal cutting. Therefore, the occurrence of tool wear directly affects the chip morphology. Up to date, a significant body of research has been conducted on the relations between chip morphology and tool wear in conventional cutting and single-point diamond turning. For example, Yao and Fang (1993) presented a novel method to explore the relationship between the chip breakability and the corresponding wear status by using neural networks techniques[6]. Kishawy & Wilcox (2003) studied the relationship between chip morphology and tool failure patterns in the cutting of hardened steel[7]. Ee et al. (2003) proposed a methodology to model the chip-curl in machining with progressively worn grooved tools[8]. Turnad et al. (2008) investigated tool wear morphology and chip segmentations in end milling of titanium alloy Ti–6Al–4V using uncoated WC-Co inserts under dry conditions[9]. Ning et al. (2008) conducted a comprehensive exploration on the correlation between chip formation and tool wear progress in ultra-fine-grained cemented carbide ball-end-milling[10]. Ebrahimi and Moshksar (2009) investigated the chips morphologies and chip/tool contact length in turning of micro-alloy and quenched-tempered steels[11]. Bhuiyan (2012) conducted a new method to explore the effect of chip generation on the tool condition using an acoustic emission method[12]. SenthilKumar (2013) performed a study on the relation between chip formation and tool wear during the drilling of carbon fiber reinforced polymer (CFRP)/titanium alloy (Ti6Al4V) stacks[13]. Meena and Mansori (2013) explored the chip morphologies at different modes of tool failure including crater wear, flank wear, chipping, breakage and built-up edge[14]. However, there has been no research on the relationship between chip morphology and tool flank wear in UPFC.

In our previous study, tool wear characteristics and their relations to cutting force were investigated[15-16]; the relation between tool wear and chip morphologies are separately explored and found that tool fractures cause ‘ridge-like’ structure on both the chip surface and machined surface while tool flank wear lead to the formation of ‘shutter-like’ structure at the tool-entry side of cutting chips[17-18]; In addition, the surface quality identification method based on cutting chip morphologies was presented initially[19]. However, there is a lack of systematically study of the tool wear evaluation approach for UPFC. This research systemically investigates tool wear evaluation approach for UPFC by using cutting chips. A tool wear evaluation procedure is designed to present the tool wear evaluation steps. This approach can evaluate both the tool failure patterns and the machined surface quality under the effects of these tool failure patterns. It is an effective tool wear evaluation approach for UPFC and other intermittent cutting processes.

2. Experiments

In the cutting experiment, both the flat cutting and depth cutting were conducted on a Precitech Freeform 705G (Precitech Inc., USA) multi-axes CNC ultra-precision fly cutting machine. The cutting tool used in this experiment was an Apex inset natural diamond tool (Apex Inc. UK) with its rake angle of -2.5°, clearance angle of 15°, and tool nose radius of 0.631mm. The workpiece material is CuZn30 and the total straight cutting distance for the flat cutting is

about 5000 m. Before the flat cutting and after every 1000 m of flat cutting, a group of depth cutting with the cutting depths of 2μm, 5μm, 10μm and 15μm were conducted. The cutting parameters are shown in Table 1.

Table 1. Cutting parameters used in this experiment

Parameters	Flat cutting	Depth cutting
Swing distance	28.35mm	28.35mm
Feed rate	44μm	50μm
Raster distance	25μm	25μm
Depth of cut	30μm	2, 5, 10,15μm

To compare the chip morphologies cut by a fresh tool and the same tool at different cutting distances, cutting chips were collected before and after every 1000 m of flat cutting and each depth cutting. The collected chips were then examined by a Hitachi TM3000 scanning electron microscope (SEM), the inspected results were reordered and used to calculate the width of flank wear. After every 1000 m flat cutting, the diamond tool was dismounted and examined by the SEM to measure the width of flank wear land.

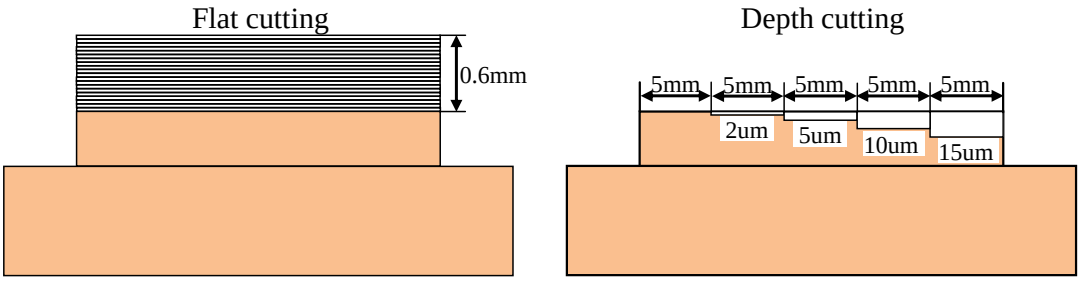

Fig. 1. Cutting strategies in flat cutting and depth cutting

3. Results and discussion

3.1. Chip formation in UPFC

In UPFC, there are two cutting strategies: horizontal cutting and vertical cutting. In horizontal cutting, the feed direction is perpendicular to the raster direction, and both of the directions for the horizontal cutting are opposite to that for the vertical cutting, as shown in Fig. 2(a-b). As a result, the formation of cutting chips can be considered as the envelopment of the tool tip profile at intervals of the tool feed rate and the raster distance, as shown in Fig. 2(c-d). Owing to the similarity of the tool wear evaluation mechanism between horizontal cutting and vertical cutting, this paper only considers the tool wear evaluation approach using cutting chips in horizontal cutting. The tool wear evaluation in the vertical cutting can be easy realized by referring the present approach.

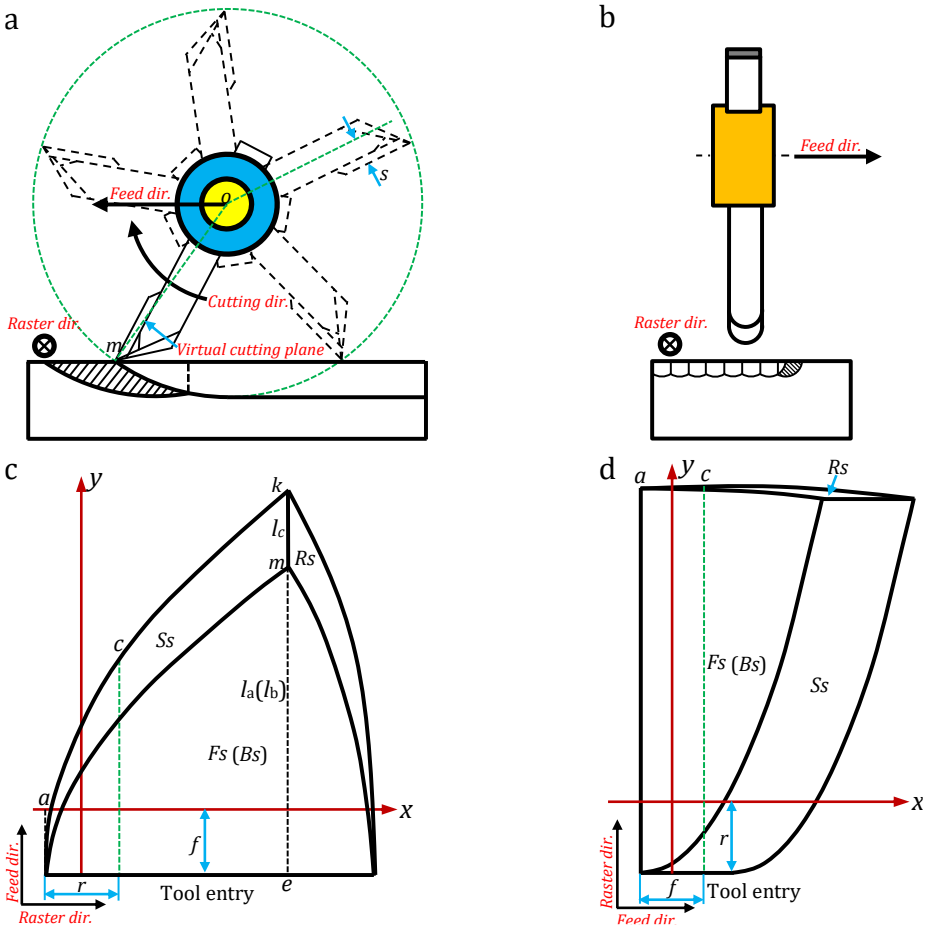

Fig. 2. Schematic of the cutting mechanism and chip formation of UPFC in (a)(c) horizontal cutting strategy, and (b)(d) vertical cutting strategy

From Fig. 2, it is found that the cutting chips in horizontal cutting are enveloped by four surfaces named: front surface (*F*s), back surface (*B*s), side surface (*S*s) and rough surface (*R*s). The equations for the four surfaces are derived as:

$$\begin{cases} Fs:\left(\sqrt{(y+f)^2+z^2}+s_w-R\right)^2+x^2=R^2 \\ Bs:\left(\sqrt{y^2+z^2}+s_w-R\right)^2+x^2=R^2 \\ Ss:\left(z+s_w-R\right)^2+\left(x+r\right)^2=R^2 \\ Rs:z=a_p-s_w \end{cases} \tag{1}$$

Where f is the feed rate; r is the raster distance; R is the tool nose radius; s_w is the swing distance, and a_p is the depth of cut.

From Fig. 2(c), it is found that along the feed direction the chip morphology is thicker at its middle (point *m*) while thinner at its two sides. The geometry feature of cutting chips makes it possible for the tool flank wear evaluation. To explore the relation between tool flank wear and cutting chip morphology, a chip thickness curve is modelled in the plane *mke* in Fig. 2(c) since the cutting edge section here has experienced the longest cutting distance.

From Eq. (1), the coordinates of point *m* and *k* are derived as:

$$\left(x_m = \sqrt{a_p(2R-a_p)} - r, \quad y_m = \sqrt{\left(\sqrt{R^2 - a_p(2R-a_p) + 2r\sqrt{a_p(2R-a_p)} - r^2} - s_w + R\right)^2 - (s_w - a_p)^2} - f \right)$$

$$\left(x_k = \sqrt{a_p(2R-a_p)} - r, \quad y_k = \sqrt{\left(\sqrt{R^2 - a_p(2R-a_p) + 2r\sqrt{a_p(2R-a_p)} - r^2} - s_w + R\right)^2 - (s_w - a_p)^2} \right)$$

From Eq. (1) and the coordinates of point *m* and *k*, the equations for the chip thickness curve are derived as:

$$\begin{cases} l_a : \left(\sqrt{(y+f)^2 + z^2} + s_w - R\right)^2 + x_m^2 = R^2 \\ l_b : z = a_p - s_w \qquad y_m \le y \le y_k \\ l_c : \left(\sqrt{y^2 + z^2} + s_w - R\right)^2 + x_m^2 = R^2 \end{cases} \tag{2}$$

Where l_a, l_b, l_c are the three segments of chip thickness curve. From Eq.(2), the chip thickness can be calculated.

3.2. Tool fractures evaluation using cutting chips

The occurrence of tool fractures is imprinted on the chip surface as a group of signatures, as shown in Fig. 3. Since cutting chips are quite thin and flatten at their tool entry area owing to the small material stacking, the signatures in this area are clear and easy to be measured precisely.

For the tool fracture evaluation, only a section of the cutting chip is valuable (chip section between line *a* and line *c* in Fig. 2), since the tool fractures imprinted on the section of chip surface are also imprinted on the machined surface. The length between line *a* and line *c* equals to the arc length of cutting edge within a raster distance, given by [17]:

$$\widehat{a} = 2R\arcsin(r/2R) \tag{3}$$

To identify the tool fractures, the distance in between and the cross-sectional profile of these signatures are measured by a 3D viewer of the Hitachi TM 3000 SEM, as is shown in Fig. 3. The measured distances and cross-sectional profile of these signatures are then parameterized to simulate the virtual cutting edge and machined surface topography. Virtual cutting edge here is an imaginary cutting edge on the virtual cutting plane, which can realize the same surface topography as the real cutting edge. While virtual cutting plane is the plane connecting the spindle axis and the tool tip point, as shown in Fig. 2(a).

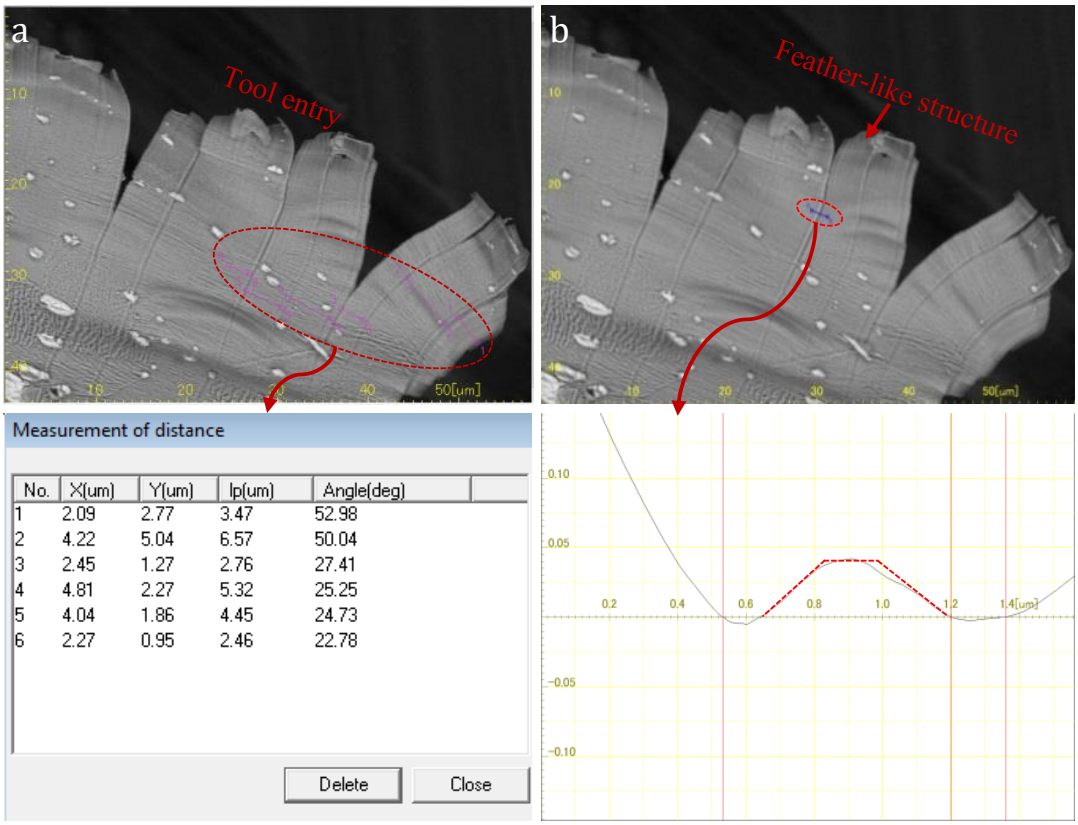

Fig. 3. (a) Signature distance measurement, and (b) signature cross-sectional profile measurement

The procedures for the signature parameterization and virtual cutting edge formation are shown in Fig. 4.

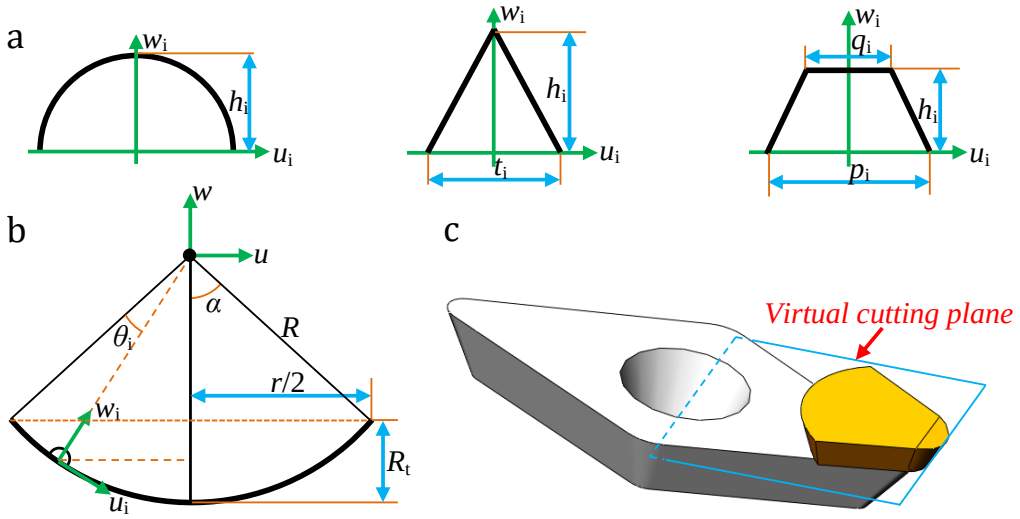

Fig. 4. Signature profile parameterization and assembly to form a virtual cutting edge

Firstly, the cross-sectional profile of a measured signature is parameterized into a geometric element, as shown in Fig. 4(a). The parameterization is based on the similarity between the signature profile and the geometric element. For example, the element in Fig. 3(b) is simplified into an isosceles trapezoid. The equations for the geometric elements are shown in Table 2.

Table 2. Equations for the geometric elements

Semi-circle	Isosceles triangle	Isosceles trapezoid
$u_i^2 + w_i^2 = h_i^2 \quad (u_i > 0)$	$\begin{cases} \frac{2u_i}{t_i} + \frac{w_i}{h_i} = 1 \quad (u_i, w_i > 0) \\ -\frac{2u_i}{t_i} + \frac{w_i}{h_i} = 1 \quad (u_i < 0, w_i > 0) \end{cases}$	$\begin{cases} w_i = \frac{2h_i}{p_i - q_i}\left(u_i + \frac{p_i}{2}\right) \quad 0 \le w_i \le h_i \\ w_i = h_i \quad -\frac{q_i}{2} \le u_i \le \frac{q_i}{2} \\ w_i = -\frac{2h_i}{p_i - q_i}\left(u_i - \frac{p_i}{2}\right) \quad 0 \le w_i \le h_i \end{cases}$

Secondly, the measured distances between any two neighbouring signatures and the parameterized geometric elements are assembled to form a virtual cutting edge. The assembly of geometry elements is completed by mathematical method.

For clarity, two coordinate systems *o*-*uw* and o_i-u_iw_i are established, as shown in Fig. 4(b).

Usually, the cutting edge is an arc, its equation is:

$$u^2 + w^2 = R^2 \tag{4}$$

The corresponding angle of the signature distance can be obtained through:

$$\theta_i = \mathrm{d}_i / R \tag{5}$$

The angle α in the Fig. 4(b) is obtained by:

$$\alpha = \arcsin\left(r / 2R\right) \tag{6}$$

Therefore, each geometric element is assembled to form the virtual cutting edge through the coordinate transformation:

$$\begin{bmatrix} u_i \\ w_i \\ 1 \end{bmatrix} = \begin{bmatrix} \cos\beta & -\sin\beta & R\sin\beta \\ \sin\beta & \cos\beta & R\cos\beta \\ 0 & 0 & 1 \end{bmatrix} \begin{bmatrix} u \\ w \\ 1 \end{bmatrix} \tag{7}$$

Where $\beta = \alpha - \sum_1^i \theta_i$ is an angle.

Thirdly, after obtaining the virtual cutting edge, the tool fractures and their locations can be identified. Since the tool fractures can also be imprinted on the machined surface, the virtual cutting edge can be used to simulate the machined surface topography based on the cutting kinematics of UPFC. The simulated topography and the side curves of the machined surface are shown in Fig. 5(a) and Fig. 5(c), which is found to be in agreement with the measured ones as shown in Fig. 5(b) and Fig. 5(d) if ignoring the mechanical errors and material flow effect.

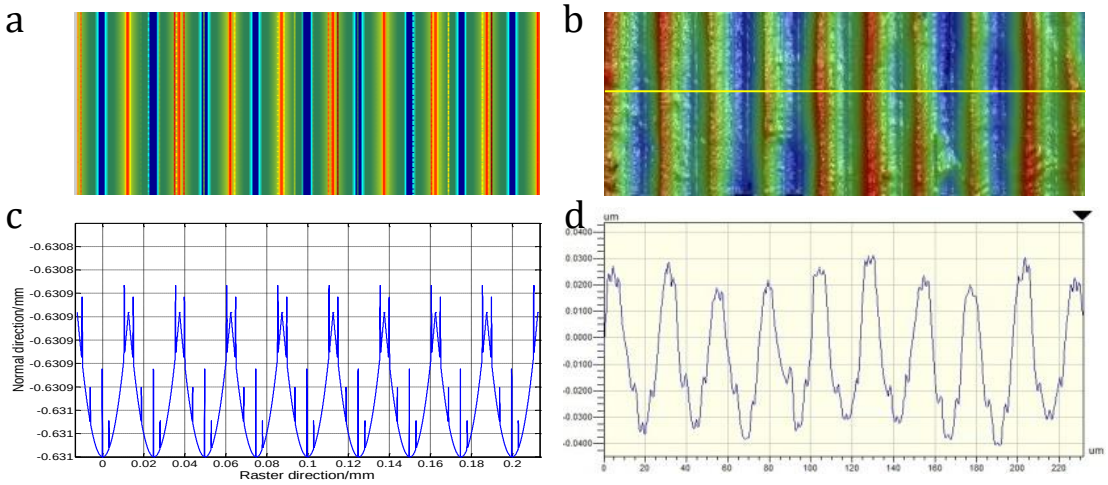

Fig. 5. Comparison between the simulated surface topography and the measured one (Wyko NT 8000)

After obtaining the simulated surface topography under tool fractures effect, the roughness, e.g. R_a, R_z and R_q, of the machined surface can be calculated from the obtained 3D data cloud. The calculated results are then used to evaluate the quality of machined surface under the effect of tool fractures.

3.3. Tool flank wear evaluation using cutting chips

After a 5000 m flat cutting, the tool flank wear and its influence on the cutting chip morphology are presented in Fig. 6. It is found that the tool flank wear makes the tool entry area of the cutting chip a louver-like structure, which is compared to a feather-like structure in Fig. 3(a-b) formed by a cutting tool with a cutting distance of 1000 m. According to the theory of minimum cutting depth, the formation of louver-like structure is thought to be caused by the comparable thickness of the cutting chips in this area and the width of tool flank wear.

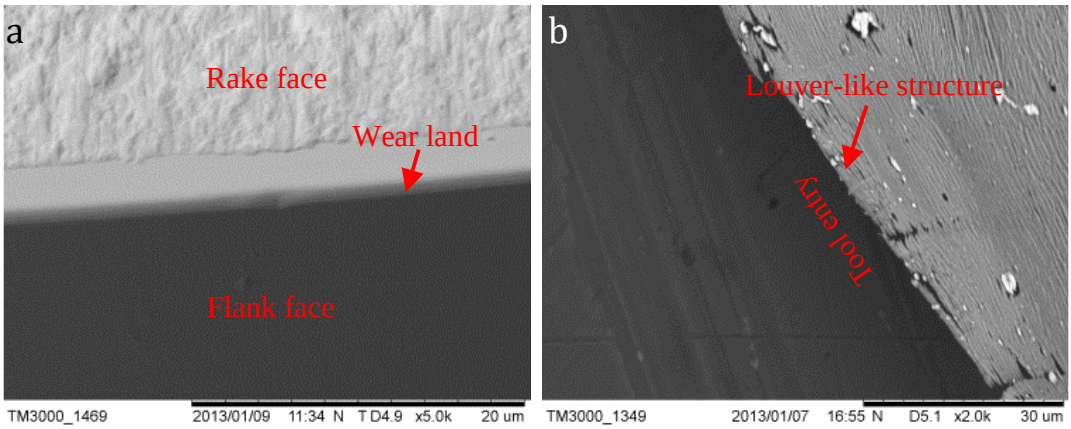

Fig. 6. (a) Tool flank wear, and (b) the louver-like structure caused by it

Under the same tool wear level the alternation of cutting depth changes the morphology of cutting chips. From Fig. 7, it is found that the tool flank wear (after 5000 m flat cutting) leads to the truncation of cutting chips at both their tool entry and tool exit areas. However, the truncation position is different at different cutting depth, e.g. the cutting chip length at cutting depth of 5μm

(Fig.7(a)) is quite shorter than that at the cutting depth of 15μm (Fig.7(b)). This is because the alteration of cutting depth changes the location of the comparable chip thickness to the width of flank wear. For a worn tool, as its cutting edge radius is comparable to a chip thickness, the chip will be truncated around this thickness. Therefore, the chip thickness at the chip truncation location can be used to identify the width of flank wear land.

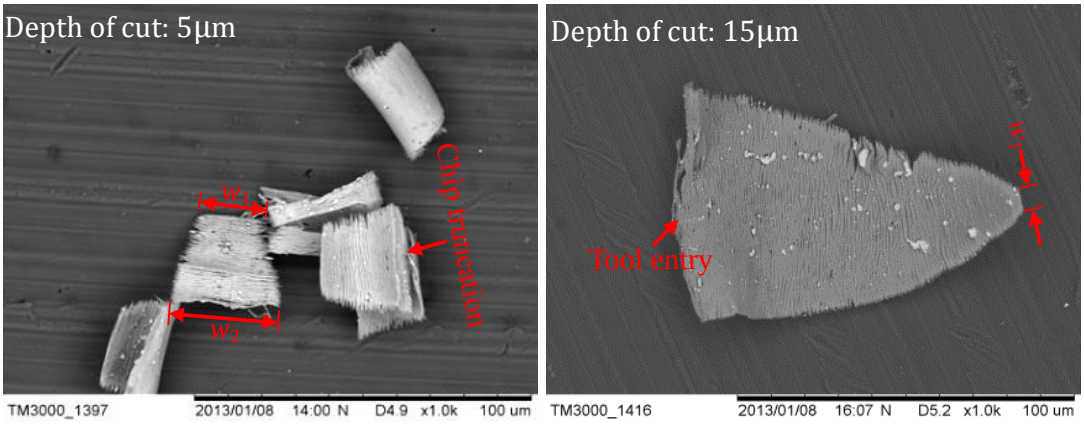

Fig. 7. Cutting chip morphologies at the cutting depth of (a) 5μm, and (b) 15μm

In UPFC, for a proper chip formation, the chip thickness must be higher than the cutting edge radius according to the theory of minimum cutting depth. The chip formation becomes difficult by decreasing the cutting depth, as seen in Fig. 8. Therefore, for accuracy and sensitivity of the identification, an optimized cutting depth and feed rate should be chosen.

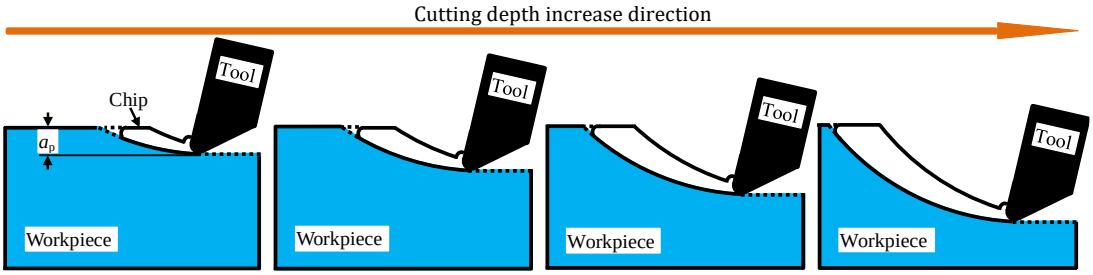

Fig. 8. Schematic illustration of the chip morphology changes with cutting depth

Based on the chip thickness curve from Eq. (1) and Eq. (2) and the relations between chip morphology and tool flank wear in UPFC, the width of flank wear can be identified. Firstly, measuring the chip width at the chip truncation locations: w_1 and w_2, as shown in Fig. 7. Secondly, calculating the chip thickness and their mean value according to the measured chip width of w_1 and w_2. Thirdly, based on the mean value of the chip thickness and the wear land angle, calculating the width of flank wear through the following equation:

$$w = c_t / \cos(\delta + \gamma) \tag{8}$$

Where w is the width of flank wear; c_t is the mean value of the chip thickness at the chip truncation; δ is the wear land angle, who is obtained by measuring the angle between rake face and wear land of cutting tools by using atomic force microscope, here it is 40.5°, as is shown in Fig.9; γ=-2.5° is the rake angle of the cutting tool.

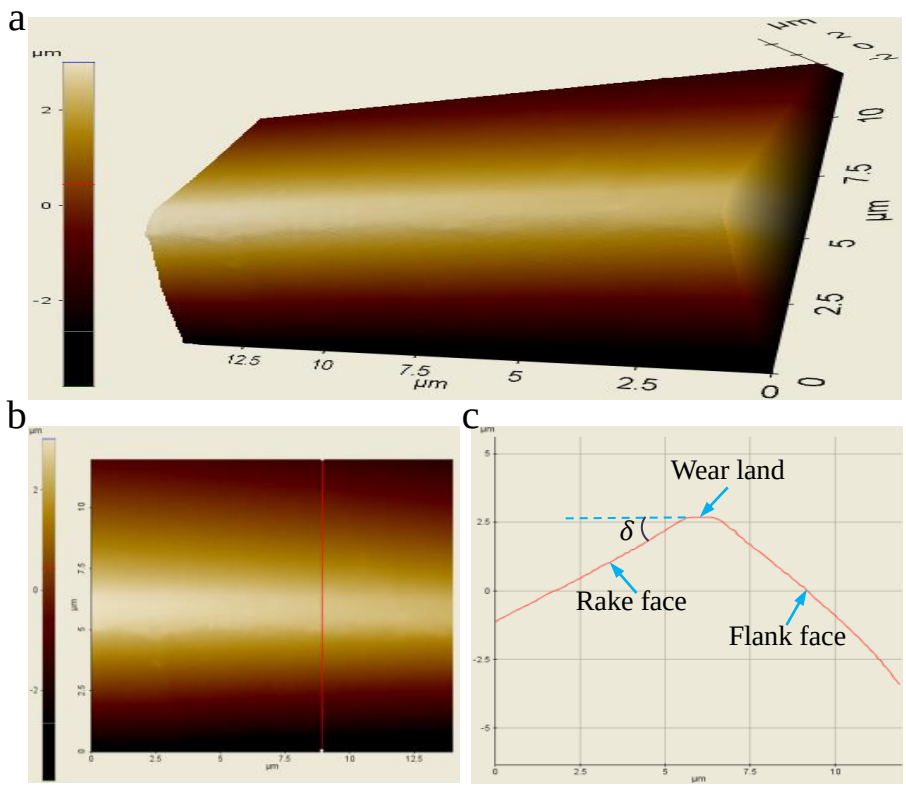

Fig. 9. Wear land angle measurement using Atomic Force Microscope (Park's XE-70)

According to the identification procedures of tool flank wear, the identified width of flank wear land at the cutting distances of 1000m, 2000m, 3000m, 4000m and 5000 m were compared with the measured ones as shown in Fig. 10(c). It is found that both the identified width and measured width of the flank wear land increase with the growing of cutting distance. However, the measured widths are a little bigger than the identified ones, which may be caused by the deviation between the width of flank wear and the chip thickness at the location of chip truncation. The deviation can be compensated by a correction factor, the modified results show a better consistency with the measured ones.

Actually, the length of truncated chips can also be used to identify the width of flank wear. However, chip length is seriously reduced during the cutting due to the material compression effect. Therefore, tool wear identification using the length of the truncated chips is not accurate. The identified results should be corrected carefully to eliminate the influence of the material compression effect.

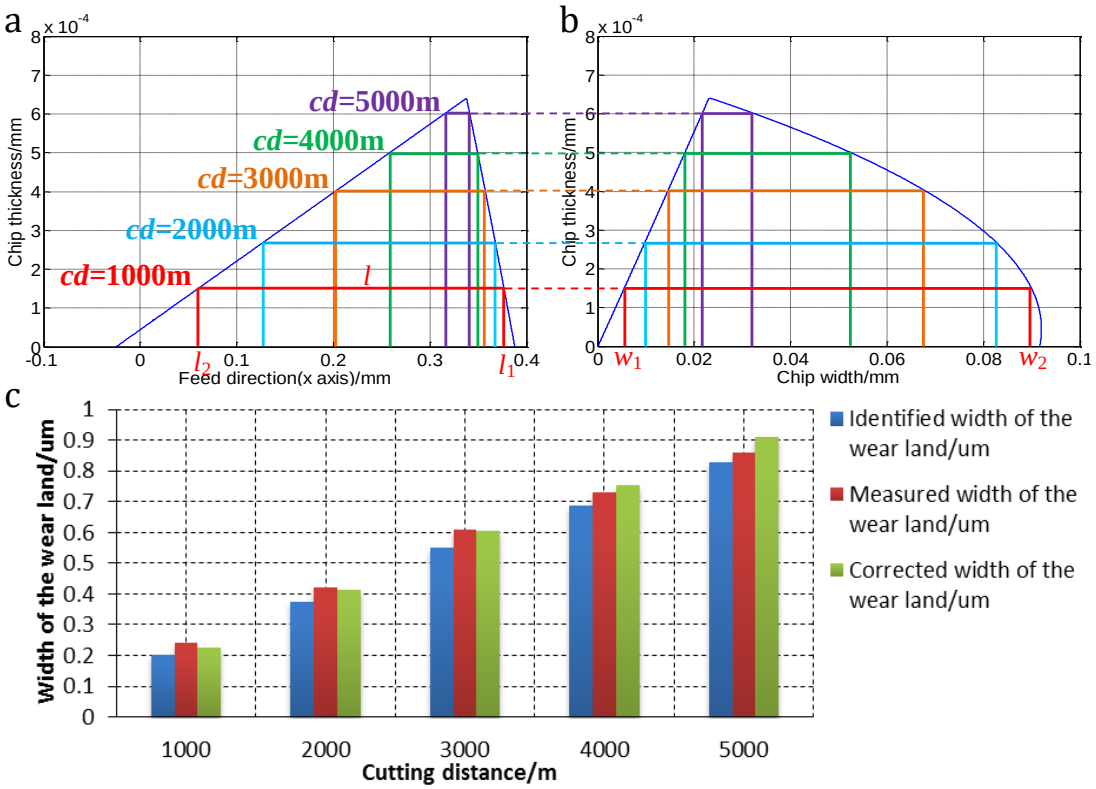

Fig. 10. Chip thickness curves used for flank wear identification

The occurrence of tool flank wear makes the cutting edge retract and forms a new cutting edge, therefore it affects the machined surface form accuracy and surface roughness. Fig. 11 shows a schematic of the cutting edge retracted and its effects on the theoretical surface roughness. Owing to the smooth wear on the cutting edge (see Fig. 6(a)), the newly formed cutting edge profile is simplified into an arc with a larger tool nose radius. Based on the geometric knowledge, the relation between the original cutting edge radius and the newly formed one is derived as [20]:

$$F(R') = \arcsin\left(\frac{R\sin\theta}{R'}\right)R' - \theta R = 0 \tag{9}$$

Where R is the original tool nose radius, R' is the newly formed tool nose radius, θ is the half angle of the wear land.

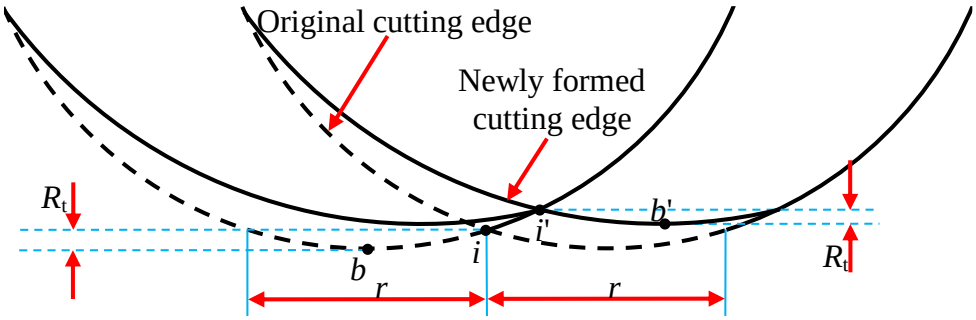

Fig. 11. Schematic of tool wear effect on surface roughness

From Eq. (9), the tool nose radius of the newly formed cutting edge can be obtained. Therefore, the surface roughness under the effect of tool flank wear, e.g. the root-mean-square roughness (R_q) and the maximum peak-to-valley height (R_t), can be calculated through [21]:

$$R_q = \sqrt{\frac{f^4}{720 s_w^2} + \frac{r^4}{720 R'^2}} \tag{10}$$

$$R_t = s_w + R' - \frac{1}{2}\left(\sqrt{4s_w^2 - f^2} + \sqrt{4R'^2 - r^2}\right) \tag{11}$$

3.4. Tool wear evaluation system

In this research, the effects of tool failure patterns on machined surface quality are successfully evaluated by using cutting chips. Fig. 12 shows the framework of a tool wear in-process evaluation system based on cutting chips. In this system, both the tool fractures and tool flank wear can be evaluated by measuring the cutting chip morphology. The system can also simulate the surface topography and predict the surface roughness under the occurrence of tool wear. Based on the predicted results, some actions can be conducted to remedy the surface quality deterioration, which include changing cutting parameters or changing tool geometry parameters.

The in-process tool wear evaluation approach based on cutting chips can effectively evaluate tool failure patterns and their effects on machined surface quality without the need to stop the cutting machine, which is a reliable approach.

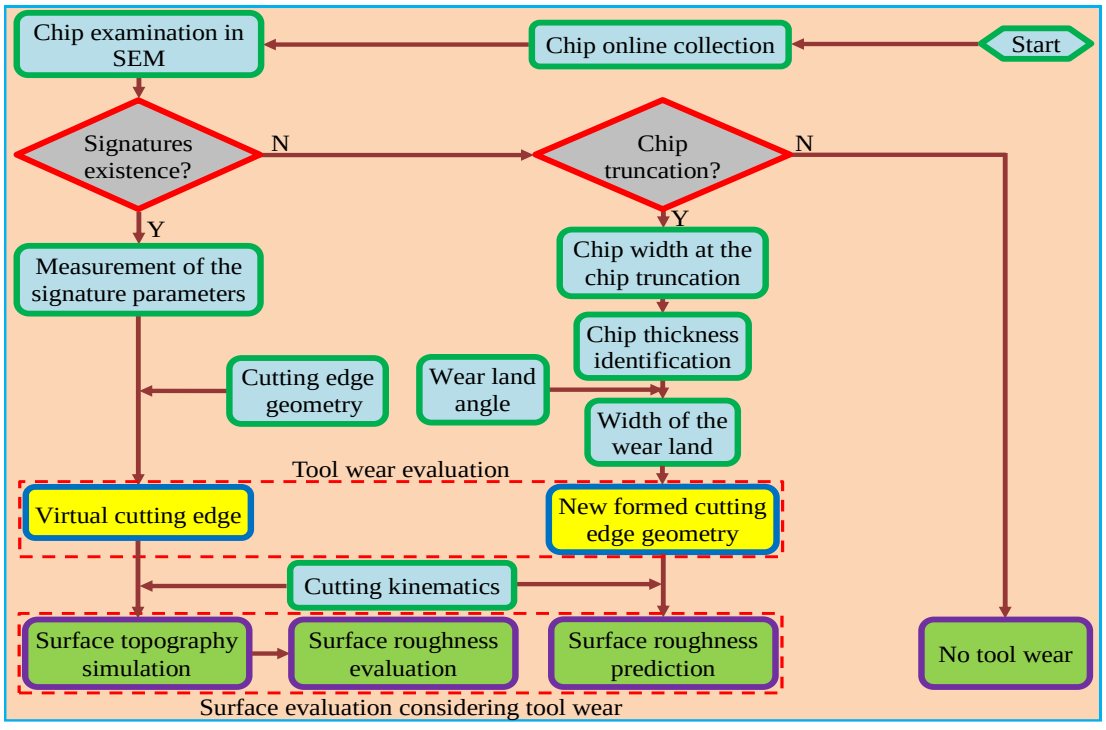

Fig. 12. Framework of the tool wear evaluation system

However, some factors affect the evaluation accuracy: firstly, material spring back during the cutting affects the measurement accuracy. Secondly, inconformity between the chip thickness at its truncation location and the width of flank wear limits the identification accuracy. The influence of these factors can be compensated for by correction factors, which will be the focus of a future study.

4. Conclusions

In the present research, tool failure patterns (tool fracture and tool flank wear) and their effects on the surface quality in ultra-precision fly cutting (UPFC) are in-process evaluated by using cutting chips. Conclusions drawn from the present study are:

(1). Tool fractures are imprinted on the chip surface as a group of signatures, both the tool fracture and surface topography can be evaluated by examining and modelling these signatures.

(2). Tool flank wear makes cutting chips truncated at the chip thickness comparable to the width of flank wear. Through identification of the chip thickness at the chip truncation location, the width of the flank wear and the surface roughness changes due to retreat of the cutting edge can be identified.

(3). A tool wear evaluation system is established to symmetrically present the procedures for tool wear and machined surface evaluation.

(4). The material property of the workpiece affects the evaluation accuracy of tool wear and surface topography.

Acknowledgement

This project is supported by National Natural Science Foundation of China (Grant No. 51505297 and 51275434).

References

[1] Yin ZQ, To S, Lee WB (2009) Wear characteristics of diamond tool in ultra-precision raster milling. International Journal of Advanced Manufacturing Technology 44(7-8):638-647

[2] Sortino M (2003) Application of statistical filtering for optical detection of tool wear. *Int J Mach Tools Manuf* 43/5: 493–49.

[3] Giusti F, Santochi M, Tantussi G (1987) On-line sensing of flank and crater wear of cutting tools. *CIRP Annals–Manufacturing Technology* 36/1:41-44.

[4] Jemielniak K, Bombiński S, Aristimuno PX (2008) Tool condition monitoring in micro-milling based on hierarchical integration of signal measures. *CIRP Annals –Manufacturing Technology* 57/1:121-124.

[5] Teti R, Jemielniak K, O'Donnell G, Dornfeld D (2010) Advanced monitoring of machining operations. CIRP Annals–Manufacturing Technology 59/2: 717-739.

[6] Yao YL and Fang XD (1993) Assessment of chip forming patterns with tool wear progression in machining via neural networks. *Int. J. Mach. Tools Manuf* 33/1: 89-102.

[7] Kishawy HA and Wilcox J (2003) Tool wear and chip formation during hard turning with self-propelled rotary tools. *Int. J. Mach. Tools Manuf* 43/4:433-439.

[8] Ee KC, Balaji AK, Jawahir IS (2003) Progressive tool-wear mechanisms and their effects on chip-curl/chip-form in machining with grooved tools an extended application of the equivalent tool face (ET) model. Wear 255/7–12:1404-1413.

[9] Turnad L, AKM NA, ANM K, Anayet U, Lajis MA (2008) Tool Wear Morphology and Chip

Segmentation in End Milling Titanium Alloy Ti–6Al–4V. CUTSE International Conference, 1-4, Miri, Sarawak, Malaysia.

[10] Ning L, Veldhuis SC, Yamamoto K (2008) Investigation of wear behavior and chip formation for cutting tools with nano-multilayered TiAlCrN/NbN PVD coating. *Int. J. Mach. Tools Manuf* 48/6:656-665.

[11] Ebrahimi A, Moshksar MM (2009) Evaluation of machinability in turning of micro-alloyed and quenched-tempered steels Tool wear, statistical analysis, chip morphology. Journal of Materials Processing Technology 209/2:910-921.

[12] Bhuiyan MSH, Choudhury IA, Nukman Y (2012) An innovative approach to monitor the chip formation effect on tool state using acoustic emission in turning. *Int J Mach Tools Manuf* 58:19-28.

[13] SenthilKumar M, Prabukarthi A, Krishnaraj V (2013) Study on tool wear and chip formation during drilling carbon fiber reinforced polymer (CFRP)/titanium alloy (Ti6Al4V) stacks. Procedia Engineering 64:582-592.

[14] Meena A, Mansori M El (2013) Specific cutting force, tool wear and chip morphology characteristics during dry drilling of austempered ductile iron (ADI). The International Journal of Advanced Manufacturing Technology 69(9-12):2833-2841.

[15] To S, Zhang G (2014) Study of cutting force in ultra-precision raster milling of V-groove. International Journal of Advanced Manufacturing Technology 75(5-8): 967-978

[16] Zhang G, To S, Zhang S (2015) Relationships of tool wear characteristics to cutting mechanics, chip formation, and surface quality in ultra-precision fly cutting. The International Journal of Advanced Manufacturing Technology DOI:10.1007/s00170-015-7483-6.

[17] Zhang G, To S, Xiao G (2014) Novel tool wear monitoring method in ultra-precision raster milling using cutting chips. Precis Eng 38/3:555-560.

[18] Zhang G, To S, Xiao G (2014) The relation between chip morphology and tool wear in ultra-precision raster milling. *Int J Mach Tools Manuf* 80–81:11-17.

[19] Zhang G, To S (2015) A novel surface quality evaluation method in ultra-precision raster milling using cutting chips. Journal of Materials Processing Technology 219:328–338.

[20] Zhang G (2014) Modelling and experimental investigation of tool wear in ultra-precision raster milling. Ph. D Thesis, The Hong Kong Polytechnic University.

[21] Cheng MN, Cheung CF, Lee WB, *et al.* (2008) Theoretical and experimental analysis of nano-surface generation in ultra-precision raster milling. *Int J Mach Tools Manuf* 48/10: 1090-1102.